

pubs.acs.org/synthbio Research Article

# Tunable and Modular miRNA Classifier through Indirect Associative Toehold Strand Displacement

Rebecca P. Chen and Wilfred Chen\*



Cite This: ACS Synth. Biol. 2022, 11, 2719–2725



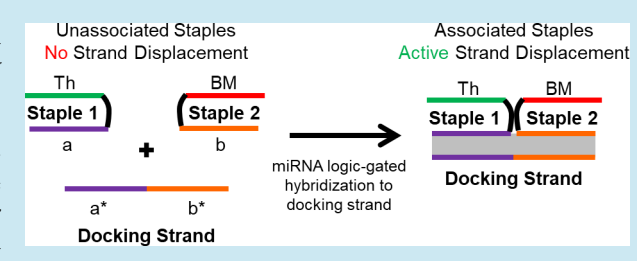
**ACCESS** 

Metrics & More

Article Recommendations

Supporting Information

ABSTRACT: The programmability of nucleic acids allows detection devices with complex behaviors to be designed de novo. While highly specific, these high-order circuits are usually sequence constrained, making their adaptability toward biological targets challenging. Here, we devise a new strategy called indirect associative strand displacement to decouple sequence constraints between miRNA inputs and de novo strand displacement circuits. By splitting circuit inputs into their toehold and branch migration regions and controlling their association through a docking strand, we demonstrate how any miRNA sequence



can be interfaced with synthetic DNA circuits, including catalytic hairpin assembly and a four-input classifier.

KEYWORDS: toehold strand displacement, miRNA, nucleic acid nanotechnology, synthetic biology

#### INTRODUCTION

MicroRNAs (miRNAs) are short (~22 nt), noncoding, and single stranded RNAs that play a crucial role in the downregulation of gene expression by hybridizing to the 3' untranslated region of target mRNA.<sup>1,2</sup> Extensive characterization in different human diseases<sup>3–8</sup> has revealed that multi-input miRNA profiles can be utilized to build highly specific cell classifiers.<sup>9–11</sup> Mature miRNAs are especially attractive for detection because they have minimal secondary structure.

DNA nanotechnology has proven to be a promising strategy for developing biomolecular "computers" that process information with Boolean-logic behavior. <sup>12,13</sup> By exploiting the concept of toehold-mediated strand displacement, DNA can be dynamically "programmed" with high sequence specificity and tunable kinetics. <sup>14,15</sup> Layering and linking strand displacement reactions with different structural components allows diverse "circuits" to be built with multiinput combinations to trigger a desired output. <sup>16,17</sup>

Most strand displacement circuits have been rationally designed de novo, and modeling approaches, such as NUPACK, offer computational methods to design optimal sequences for desired behaviors. While these advances accelerate the design of synthetic DNA circuitry with ideal behavior, challenges remain in adapting them for miRNA, whose short length means no sequence flexibility in targeting. Strict sequence constraints often compromise device function and efficiency. Linear strand displacement cascades, with limited secondary structure, have thus far seen the most success with biological targets. However, DNA devices with more complex elements, such as structural hairpin features, had more limited success. This is particularly true for amplification circuits based on catalytic hairpin assembly (CHA) (Figure

S1), where the fidelity and integrity of hairpin formation is easily affected by sequence constraints. Unstable or improper hairpin folding can lead to slower kinetics and increased background leak. In this paper, we sought to relax the sequence constraints for practical application toward miRNA-gated CHA circuits.

## ■ RESULTS AND DISCUSSION

To achieve multi-input CHA, we apply the concept of associative strand displacement, which splits the input strand into two components between the toehold and branch migration regions. Each component by itself is incapable of strand displacement. However, when brought together by a docking strand, association of the split components activates strand displacement. The concept of associative toehold circuits has been previously demonstrated through three-way junctions, in which the split components hybridize to each other.<sup>22–25</sup> Here, we build upon these works and introduce a docking strand to create a four-way junction for associative strand displacement. This allows for complete sequence independence between the two split components, and thus custom tuning of each toward its respective miRNA target.

Using this strategy, we propose a new approach to design multi-input, miRNA-driven CHA circuits by using an indirect associative strand displacement scheme (Figure 1). The split

Received: March 7, 2022 Published: July 11, 2022





ACS Synthetic Biology pubs.acs.org/synthbio Research Article

# Indirect Associative Catalyst Scheme (AND-Gate)

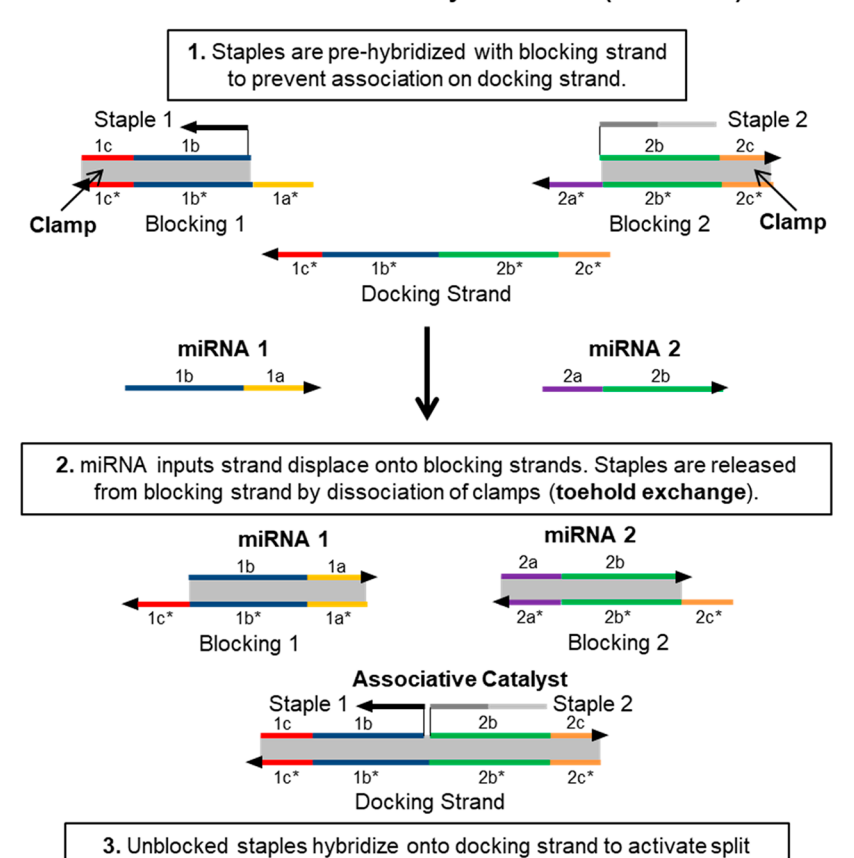


Figure 1. Indirect associative catalyst scheme (AND-Gate). Step 1. Staple strands are prehybridized to blocking strands to prevent initial hybridization to docking strand. Clamps, domains (1c) and (2c), are added to increase duplex stability and limit competitive hybridization. Step 2. MicroRNA inputs (22 nt in total length) displace the blocking strands through toehold domains (1a) and (2a), which are 6–8 nt in length. Step 3. Unblocked staples hybridize to the docking strand to activate the split catalyst. Both miRNA inputs must be present for activation to occur. Refer to Figure S4a for alternative reaction pathways.

catalyst. Both miRNA inputs must be present for activation to occur.

catalyst components are prehybridized with blocking strands to prevent association with the docking strand. The presence of target miRNAs triggers strand displacement and release of the split catalyst staples, allowing reactivation on the docking strand. Multi-input CHA is demonstrated for the first time with AND, NOT, and NOTAND logic behaviors. Furthermore, the strategy is generalized beyond CHA into a four-input miRNA classifier. This modular method allows for the elegant interfacing of endogenous miRNA targets with de novo nucleic acid devices.

The design principle of the split associative catalyst was first investigated by using a fluorophore/quencher reporter duplex (Figure S1). The reconstitution of the split catalyst staples on the docking strand results in a hairpin assembly that exposes the toehold (2\*) domain on the H1 strand, which displaces the fluorophore strand from the quencher strand. Fluorescence measurements were normalized by subtracting the signal of the CHA hairpins alone. Since short miRNAs have a limited length, we first investigated the effect of hybridization length to the docking strand in our split catalyst design (Figure S2). Increasing the docking length improved hybridization and formation of the split catalyst, leading to improved kinetics with a maximum initial rate achieved using a 16 nt docking region, while a 10 nt version offered almost no activation (Figure S2a). This guided our design moving forward in using

6 nt of the miRNA for the toehold and the remaining 16 nt for branch migration.

The split location can also affect the conditional nature of catalyst strand activation. The leak observed from staple 1 alone in a halfway split catalyst design (Figure S2b) was unsurprising since it contains not only the toehold region but also a significant portion of the branch migration sequence. To eliminate this leak, the split location was shifted closer to the junction between the toehold and branch migration domains, denoted location (0). As the split location approaches this junction, decreasing leak is observed, and at the (+1) location, where staple 1 includes 1 nt of the branch migration region, no leak was observed even over 12 h (Figure 2), which was used for future experiments. While the best split catalyst is three times slower than the unsplit "1-strand" catalyst positive control, the CHA reaction was still complete quickly within 90 min (Figure S3).

Next, we proceeded to interface the split catalyst with miRNA sequences. The catalyst region was kept constant, while the docking region was adapted for miRNA compatibility. Because the docking region does not have structural constraints, its sequence is easily exchangeable. Using this modularity, a new indirect associative strand displacement AND-gate scheme (Figure 1) was developed using two miRNAs as inputs to trigger strand displacement of blocking

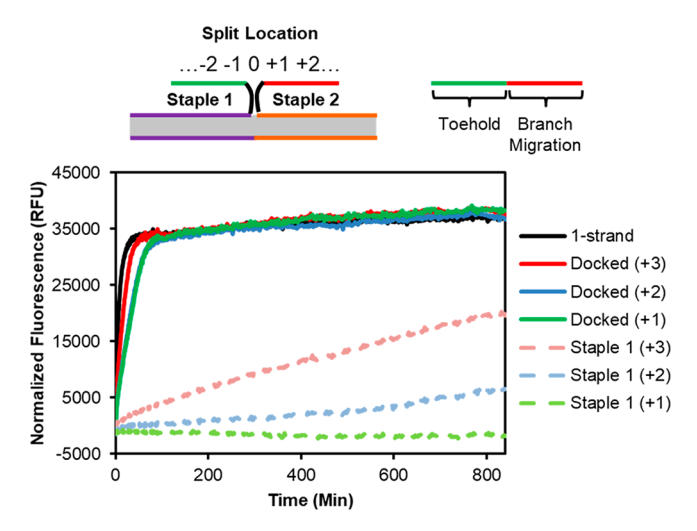


Figure 2. Optimization of split location. The location at which the catalyst strand was split was varied at the (+1), (+2), and (+3) locations. Location (0) is the junction between the toehold and branch migration domain. Staple 1 by itself was still capable of initiating hairpin assembly in the (+3) and (+2) locations. At location (+1), no staple 1 leak is observed.

strands from staples through toehold exchange (Figure S4b). <sup>14</sup> The unblocked staples can then hybridize to the docking strand for associative catalyst formation. In this scheme, there is nontrivial competition between the miRNA and the staples for the docking strand due to shared complementarity in domains (1b) and (2b) (Figure S4a). To combat this competition, clamps <sup>16,26</sup> (made up of Gs and Cs), domains (1c) and (2c), were added to the end of the staples to provide greater complementarity than the miRNA for the docking strand. More generally, the short and unstructured nature of miRNAs lends the staples and blocking strands to anneal at high fidelity when prepared as described in the methods.

To investigate how the clamp could impact overall kinetics and leak, the clamp length was varied. A 6 nt toehold and 16 nt branch migration region were utilized for each miRNA. When only the docking strand and staples were mixed, clamp length had little effect on CHA kinetics (Figure S5a), as the absence of miRNA meant no competitive hybridization. Similarly, when the docking strand and blocked staples were combined, no leak was observed regardless of clamp length (Figure S5b). Next, the docking strand was mixed with the staples (without blocking strands) and miRNA to study competitive hybridization (Figure S5c). For all clamp lengths, CHA was slower in the presence of miRNA. Without a clamp, virtually no CHA was observed, but with increasing clamp length, CHA kinetics increased as staples outcompeted miRNA for the docking strand.

After confirming the split catalyst can be stably maintained on the docking strand using a 6 nt clamp even in the presence of the competing miRNAs, we tested the use of miRNAs to execute the full AND-gate circuit. The docking strand and blocked staples were combined with the two miRNA targets (Figure S5d). The 5 nt clamp was found to be optimal, with clamp lengths both longer and shorter having slower kinetics. Despite the benefits of the longer clamp (6 nt and 7 nt) in minimizing miRNA competition to the docking strand, the clamp is too long for toehold exchange to favor efficient release of the staple. However, for shorter clamps (3 nt and 0 nt), increased miRNA competition reduced CHA kinetics despite

allowing for efficient staple release. In this study, GC clamp length has been used as a heuristic design rule to demonstrate the balance between minimizing miRNA competition and having efficient release of the staple. Optimal clamp length will also depend on the sequence composition of the clamps, with lower GC composition requiring longer clamps.

Using the 5 nt clamp, the AND-gated CHA was tested against the full truth table, and CHA was only observed when both miR-122 and miR-21 were present (Figure 3). Hairpin

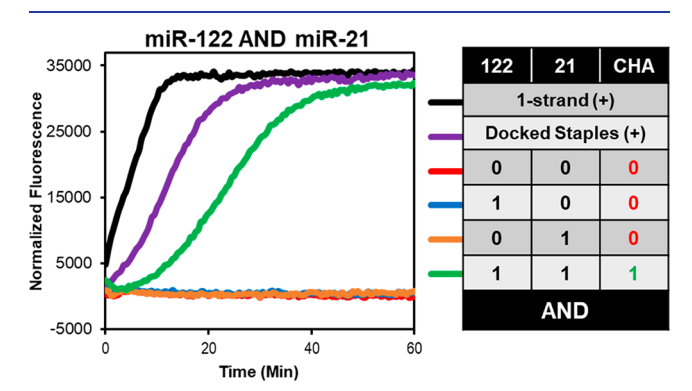


**Figure 3.** Response of AND-gated CHA. CHA fluorescence amplification was observed only in the presence of miR-21 AND miR-122.

assembly is slightly slower in reaching completion (~60 min), but only twice as long as the docked staples positive control (staples prehybridized to docking strand). We next designed a NOT-gated CHA circuit (Figure 4a). No clamp is necessary here as there is no competing hybridization event. Since strand displacement kinetics are highly dependent on the toehold length and strand concentration, 27 we evaluated the threshold of the NOT-gate using 6 nt and 8 nt toehold designs (Figure 4b). With the 6 nt toehold, CHA was not turned off effectively at the lower concentration of miR-141. However, the 8 nt toehold design was able to turn off CHA after a small initial increase in fluorescence, since strand displacement to disrupt the associative catalyst occurred faster. For both designs, adding 4-fold more miR-141 was sufficiently high enough concentration to cause disassembly of all initial associative catalysts instantaneously. This provides a framework for utilizing toehold length as way to tune threshold concentrations required for NOT-gated behavior. This is particularly important since many miRNAs of interest may be downregulated but not completely absent. Thresholding offers a way to tune and capture "low" states to execute "NOT" behavior.

The AND-gate and NOT-gate designs were combined to create a NOTAND-gated CHA circuit (Figure 5a). In this scheme, staple 1 is prehybridized to the docking strand and staple 2 is prehybridized to a blocking strand. A functional split catalyst is formed only if miRNA 1 is absent and miRNA 2 is present. A NOT miR-141 AND miR-21 design was tested against all input combinations. Only in the absence of miR-141 and presence of miR-21 did CHA occur (Figure 5b). When both miR-141 and miR-21 were added there was no initial leak, unlike the NOT miR-141 design. The time delay for strand displacement of staple 2 from the blocking strand eliminates initial catalyst activity before the NOT displacement is completed.

Using the AND/NOT indirect associative strand displacement schemes, we further developed a four-input miRNA

ACS Synthetic Biology pubs.acs.org/synthbio Research Article

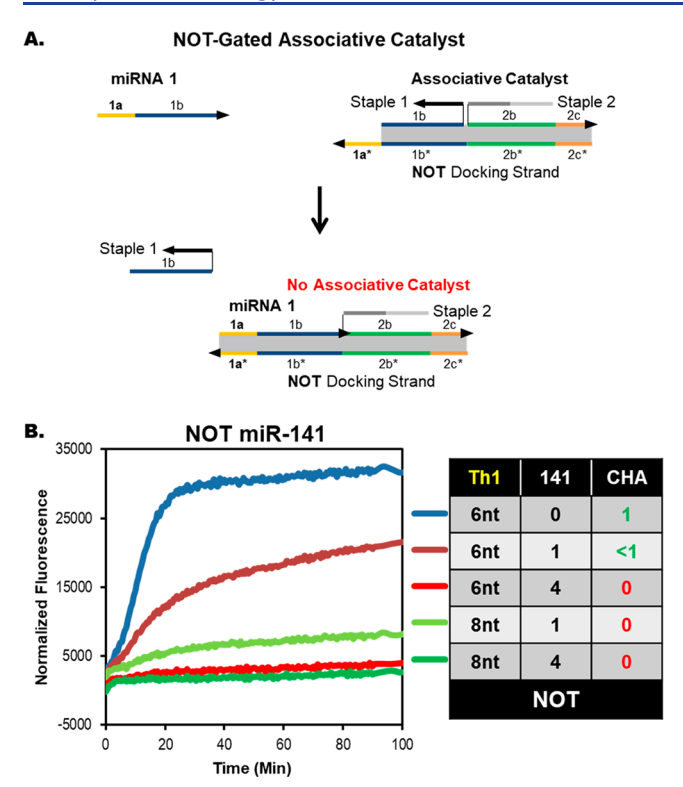


**Figure 4.** NOT-gated CHA. (a) Schematic of NOT-gated associative catalyst. The presence of NOT-gated miRNA displaces Staple 1 from the docking strand through toehold (1a), deactivating the associative catalyst. (b) Fluorescence of the NOT-gated CHA circuit. Toehold (1a) length of 6 nt and 8 nt is shown to modulate the miRNA (miR-141) threshold concentration of the NOT-gate.

classifier based on a two-input circuit from our previous study.<sup>28</sup> This circuit can be easily expanded to four inputs by splitting each of the original inputs at their toehold and branch migration junctures. Each split associative input was NOTAND-gated by two miRNA targets (Figure 6a). The miRNA combination tested has been previously used to successfully distinguish HeLa cells from six other human cell lines. 10 Increasing the number of miRNA markers used in a classifier allows for improved selectivity of different cell types. In this case, expanding from miR-21 AND miR-17 to also include NOT miR-141 and NOT miR-146 can further distinguish cancer HeLa cells from healthy pancreatic islet and podocyte cell types. 10 All possible Boolean combinations were challenged in the 4-input classifier, and an optimal reaction end point of 6 h was chosen for fluorescence measurement (Figure 6b). Only the desired miRNA combination resulted in a significant 70% drop in fluorescence, while other conditions had minimal leak (Figure 6c). We envision that a patient RNA sample can be mixed with the circuit in a one-pot reaction, where the measured fluorescence is converted to a simple binary diagnostic output without extensive data processing.

Furthermore, the panel of miRNA assayed can be easily expanded in the same pot by using orthogonal fluorophores in parallel. Alternatively, a complete set of 16 differentially labeled versions of the classifier, where the fluorophore and quencher are placed on various strands to detect different strand displacement events, could also be used to elucidate the exact condition of the sample. Our study focused on novel modalities for conditionalizing CHA and not necessarily

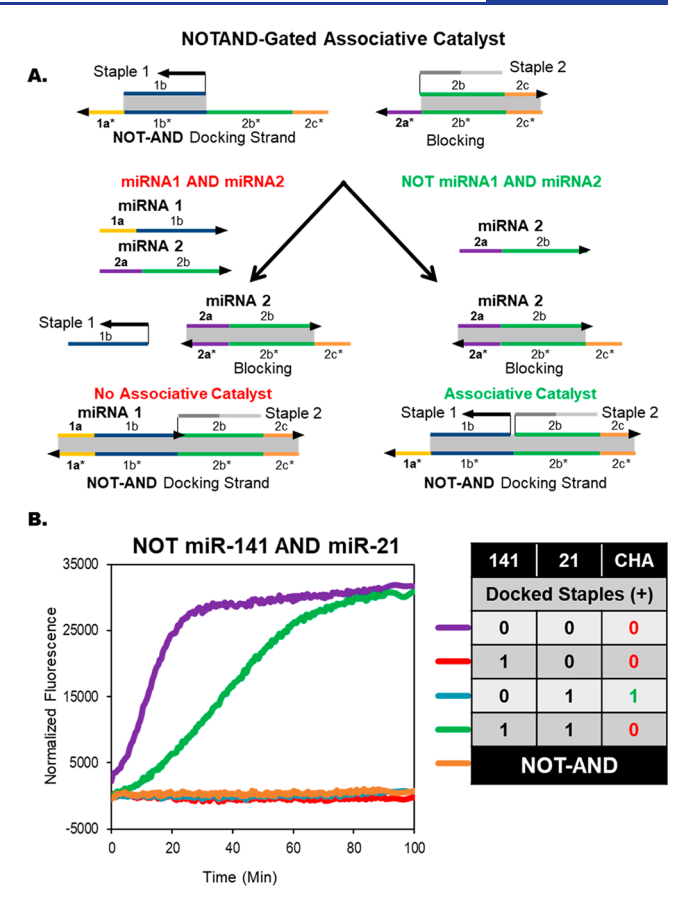


**Figure 5.** NOTAND-gated CHA. (a) Schematic of NOTAND-gated associative catalyst. The presence of miRNA 1 displaces staple 1 from the docking strand. miRNA 2 triggers the release of the staple 2 from the blocking strand. Only the right combination yields the split associative catalyst. (b) Fluorescence of the NOTAND-gated CHA circuit. Only in the absence of miR-141 and presence of mir-21 is increased fluorescence from CHA observed.

circuit sensitivity. However, a recent study demonstrated that when coupled with an electrochemical output, CHA can achieve femtomolar sensitivity, implicating the potential of utilizing CHA for detecting miRNA in clinical samples. Cui et al. successfully detected 1.8 fmol of miR-21 from 5  $\mu$ g of total RNA extracted from MCF-7 cells, supporting the feasibility of sensitive CHA within complex RNA samples.

In this study, an indirect associative strand displacement concept is used to achieve miRNA logic-gated classifiers without sequence constraints. Toehold length and clamp length serve as tunable parameters for adapting any miRNA of interest. Various indirect associative catalyst designs were executed with logic-gated behavior, including AND, NOT, and NOTAND designs. This powerful strategy is generalizable to any strand displacement reaction and provides an initial framework for creating simple diagnostic assays. Beyond cellfree sensing applications, as the field makes progress in overcoming current intracellular delivery hurdles, associative strand displacement could serve as a strategy for creating miRNA-responsive devices that probe and control cellular behavior of live cells for in vivo applications.<sup>30</sup> However, additional challenges beyond delivery include stability and halflife of the circuit in the cytosol, how to ensure all circuit components are delivered, and how the crowded intracellular

ACS Synthetic Biology pubs.acs.org/synthbio Research Article

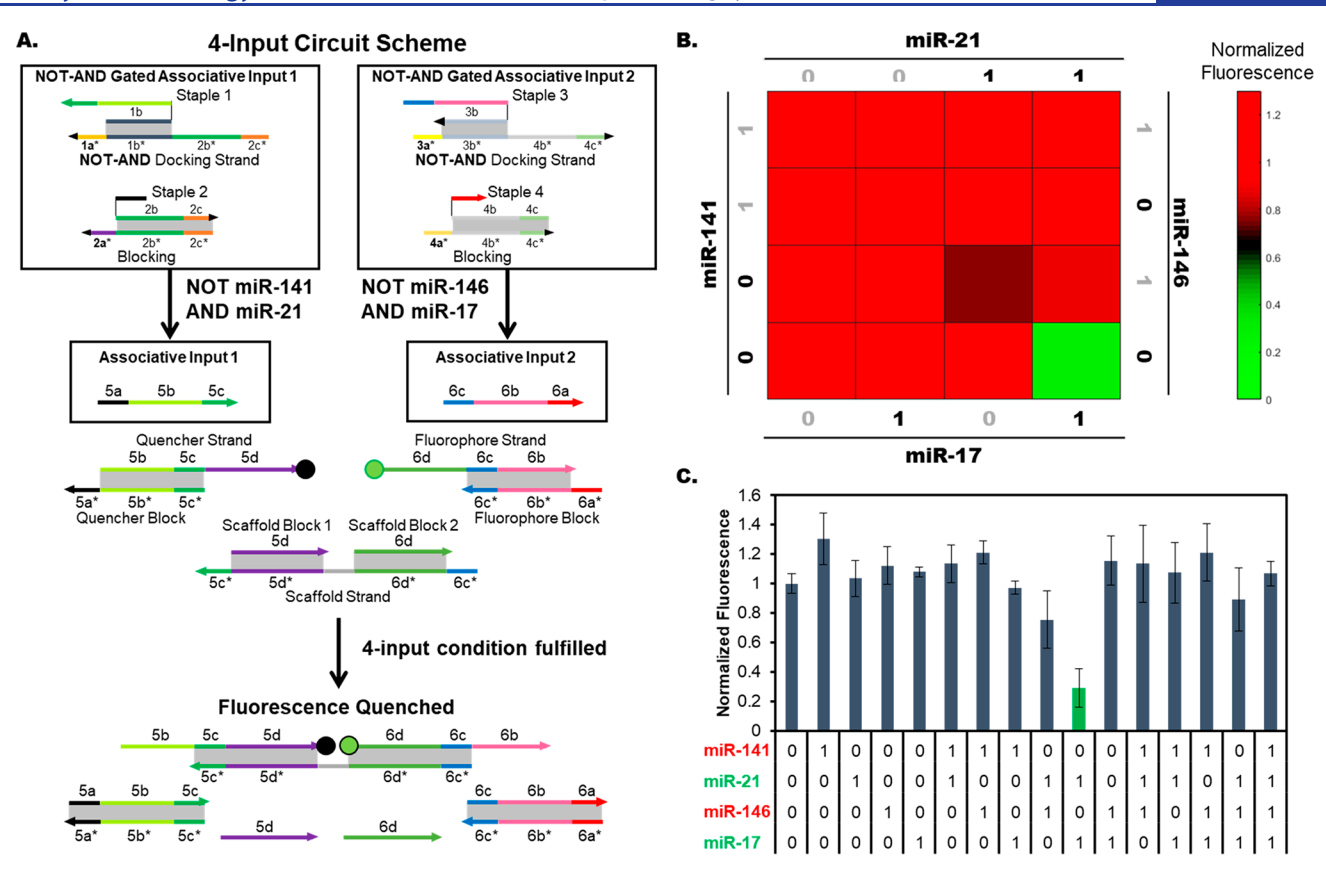


Figure 6. Four-input miRNA classifier. (a) Each associative input is controlled by a NOTAND-gate. Associative input 1 and associative input 2 trigger strand displacement of a quencher strand and a fluorophore strand onto the scaffold strand, respectively. Only the correct combination of all four miRNA will result in fluorescence quenching. (b) Heat map representation of normalized fluorescence for the full logic table at 6 h. Fluorescence was normalized between the no input condition (set at 1) and the fluorophore and quencher prehybridized to the scaffold strand (set at 0). Only the correct four-input condition results in a quenched signal (green). (c) Bar graph representation of normalized fluorescence at 6 h for full logic table. The positive input condition (green) is statistically significant from all other input conditions with at least  $p \le 0.05$ , denoted by \*, and calculated by an unpaired Student's t test. Error bars represent the standard deviation of t = 3 biological replicates.

environment affects the kinetics and output signal of the circuit.

# METHODS

**Materials.** DNA oligos were purchased from Integrated DNA Technologies with standard desalting unless otherwise indicated. Oligo sequences along with specific strand modifications are listed in Table S1. All DNA was reconstituted in hybridization buffer (20 mM Tris, 150 mM NaCl, 5 mM MgCl<sub>2</sub>, pH 7.4). DNA mimics of miRNA targets were used in this study.

**Preparation of DNA Complexes.** Prehybridized complexes were prepared by heating followed by slow cooling in a thermocycler (BioRad) as follows. Complexes were prepared in hybridization buffer and heated to 95 °C for 10 min. Prehybridization was conducted by mixing the blocking strand with 1.1× excess of the staple strand to enhance duplex formation. Prehybridization buffer also contains NaCl and MgCl<sub>2</sub> to further stabilize hybridization. Afterward the solution was slowly cooled to 4 °C at a rate of 0.1 °C/sec. DNA complexes were stored at 4 °C overnight before use. H1, H2, and the reporter duplex were prepared separately at 30  $\mu$ M. Blocked staples and/or docking strand complexes were prepared at 10× the final concentration. For the four-input miRNA classifier, all complexes were prepared at 10× the final concentration.

Circuit Running Conditions. All CHA experiments were run at 37 °C. A ratio of 1:4 was used for catalyst components to hairpins. The fluorophore/quencher reporter duplex, H1, and H2 were all used at a final concentration of 1  $\mu$ M. The 1strand catalyst, various associative catalyst staples, and docking strand were used at 250 nM. The blocking strands were added in 1.2× (300 nM) excess of the staples, and the inputs were added in 1.2× (360 nM for AND, 300 nM for NOT) excess of the blocking strands. The final concentration of miRNA input (300 nM) was denoted with the Boolean logic value of 1. For the NOT-gate a logic value of 4 was also tested and is equivalent to 1200 nM. In general, a master mix of reporter duplex, H1, and H2 was first prepared and added to wells. Next, various logic gate components were added. The miRNA inputs were added last and then immediately assayed on the plate reader.

The four-input miRNA classifier was run at 25 °C. The blocked central scaffold complex was prepared with 400 nM of scaffold strand and 800 nM of blocking strands. The blocked fluorophore and blocked quencher duplexes were prepared at 750 nM of blocking strand and 500 nM of fluorophore or quencher strand. NOTAND classifier components are prepared at 900 nM for docking and staple strands. For staple blocking strands, 1080 nM was used. The miRNA inputs were added in 2-fold (1800 nM for NOT and 2160 nM for AND),

corresponding to the Boolean value of 1. Data plotted in Figure 6 is at the optimal end point of 6 h.

Fluorescence Measurements of DNA Circuits. For the characterization of associative catalyst designs, samples were set up at  $100~\mu\text{L}$  per well in black 96-well plates. Fluorescence measurements were taken using the Synergy H4 (BioTek) plate reader at a sensitivity setting of 85. Excitation and emission wavelengths of 470 and 520 nm were used to measure FAM fluorescence, respectively. Fluorescence readings were taken every 30 s for the first 2 h and afterward every 2 min. For the four-input miRNA classifier, 25  $\mu$ L samples were set up in clear PCR tubes and caps for optical reactions. Fluorescence measurements were taken on the FAM channel using a qPCR machine (BioRad, CFX96). Measurements were taken every 5 min.

## ASSOCIATED CONTENT

# **5** Supporting Information

The Supporting Information is available free of charge at https://pubs.acs.org/doi/10.1021/acssynbio.2c00124.

All oligo sequences used in this study (Table S1); CHA reaction pathway and detection scheme (Figure S1); effect of docking hybridization length (Figure S2); optimization of split location (Figure S3); reaction pathway of competitive hybridization and mechanism of toehold exchange (Figure S4); effect of varying GC clamp length on indirect associative catalyst AND-gate design (Figure S5) (PDF)

## AUTHOR INFORMATION

#### **Corresponding Author**

Wilfred Chen — Department of Chemical and Biomolecular Engineering, University of Delaware, Newark, Delaware 19716, United States; orcid.org/0000-0002-6386-6958; Email: wilfred@udel.edu

### **Author**

Rebecca P. Chen — Department of Chemical and Biomolecular Engineering, University of Delaware, Newark, Delaware 19716, United States

Complete contact information is available at: https://pubs.acs.org/10.1021/acssynbio.2c00124

#### **Author Contributions**

R.P.C. and W.C. conceived the project. R.P.C. designed experiments, performed the experiments, analyzed the data, and wrote the manuscript. W.C. designed experiments, analyzed the data, and wrote the manuscript. Both authors discussed the results and commented on the manuscript.

#### Notes

The authors declare no competing financial interest.

### ACKNOWLEDGMENTS

We would like to acknowledge the funding support from NSF (CBE1803008, MCB1817675, and MCB2013991).

## REFERENCES

- (1) Carthew, R. W. Gene regulation by microRNAs. Current Opinion in Genetics & Development 2006, 16, 203–208.
- (2) Bartel, D. P. MicroRNAs: Target Recognition and Regulatory Functions. *Cell* **2009**, *136*, 215–233.

- (3) Kozomara, A.; Birgaoanu, M.; Griffiths-Jones, S. miRBase: from microRNA sequences to function. *Nucleic Acids Res.* **2019**, *47*, D155–D162
- (4) Condrat, C. E.; Thompson, D. C.; Barbu, M. G.; Bugnar, O. L.; Boboc, A.; Cretoiu, D.; Suciu, N.; Cretoiu, S. M.; Voinea, S. C. miRNAs as Biomarkers in Disease: Latest Findings Regarding Their Role in Diagnosis and Prognosis. *Cells* **2020**, *9*, 276.
- (5) Li, Y.; Kowdley, K. v. MicroRNAs in Common Human Diseases. Genomics, Proteomics & Bioinformatics 2012, 10, 246–253.
- (6) Paul, P.; Chakraborty, A.; Sarkar, D.; Langthasa, M.; Rahman, M.; Bari, M.; Singha, R. K. S.; Malakar, A. K.; Chakraborty, S. Interplay between miRNAs and human diseases. *Journal of Cellular Physiology* **2018**, 233, 2007–2018.
- (7) Tong, A. W.; Nemunaitis, J. Modulation of miRNA activity in human cancer: a new paradigm for cancer gene therapy? *Cancer Gene Ther.* **2008**, *15*, 341–355.
- (8) Lu, M.; Zhang, Q.; Deng, M.; Miao, J.; Guo, Y.; Gao, W.; Cui, Q. An Analysis of Human MicroRNA and Disease Associations. *PLoS One* **2008**, *3*, No. e3420.
- (9) Seelig, G.; Soloveichik, D.; Zhang, D. Y.; Winfree, E. Enzyme-Free Nucleic Acid Logic Circuits. *Science* **2006**, *314*, 1585–1588.
- (10) Xie, Z.; Wroblewska, L.; Prochazka, L.; Weiss, R.; Benenson, Y. Multi-Input RNAi-Based Logic Circuit for Identification of Specific Cancer Cells. *Science* **2011**, 333, 1307–1311.
- (11) Mohammadi, P.; Beerenwinkel, N.; Benenson, Y. Automated Design of Synthetic Cell Classifier Circuits Using a Two-Step Optimization Strategy. *Cell Systems* **2017**, *4*, 207–218.
- (12) Zhang, D. Y.; Seelig, G. Dynamic DNA nanotechnology using strand-displacement reactions. *Nat. Chem.* **2011**, *3*, 103–113.
- (13) Yin, P.; Choi, H. M. T.; Calvert, C. R.; Pierce, N. A. Programming biomolecular self-assembly pathways. *Nature* **2008**, *451*, 318–322
- (14) Zhang, D. Y.; Winfree, E. Control of DNA Strand Displacement Kinetics Using Toehold Exchange. *J. Am. Chem. Soc.* **2009**, *131*, 17303–17314.
- (15) Xiao, M.; Lai, W.; Man, T.; Chang, B.; Li, L.; Chandrasekaran, A. R.; Pei, H. Rationally Engineered Nucleic Acid Architectures for Biosensing Applications. *Chem. Rev.* **2019**, *119*, 11631–11717.
- (16) Qian, L.; Winfree, E. Scaling Up Digital Circuit Computation with DNA Strand Displacement Cascades. *Science* **2011**, 332, 1196–1201.
- (17) Qian, L.; Winfree, E.; Bruck, J. Neural network computation with DNA strand displacement cascades. *Nature* **2011**, *475*, 368–372.
- (18) Zadeh, J. N.; Steenberg, C. D.; Bois, J. S.; Wolfe, B. R.; Pierce, M. B.; Khan, A. R.; Dirks, R. M.; Pierce, N. A. NUPACK: Analysis and design of nucleic acid systems. *J. Comput. Chem.* **2011**, 32, 170–173.
- (19) Wolfe, B. R.; Porubsky, N. J.; Zadeh, J. N.; Dirks, R. M.; Pierce, N. A. Constrained Multistate Sequence Design for Nucleic Acid Reaction Pathway Engineering. *J. Am. Chem. Soc.* **2017**, *139*, 3134–3144
- (20) Hemphill, J.; Deiters, A. DNA Computation in Mammalian Cells: MicroRNA Logic Operations. *J. Am. Chem. Soc.* **2013**, *135*, 10512–10518.
- (21) Li, B.; Ellington, A. D.; Chen, X. Rational, modular adaptation of enzyme-free DNA circuits to multiple detection methods. *Nucleic Acids Res.* **2011**, *39*, e110–e110.
- (22) Ang, Y. S.; Tong, R.; Yung, L.-Y. L. Engineering a robust DNA split proximity circuit with minimized circuit leakage. *Nucleic Acids Res.* **2016**, *44*, e121–e121.
- (23) Genot, A. J.; Bath, J.; Turberfield, A. J. Combinatorial Displacement of DNA Strands: Application to Matrix Multiplication and Weighted Sums. *Angew. Chem., Int. Ed.* **2013**, 52, 1189–1192.
- (24) Li, F.; Lin, Y.; Le, X. C. Binding-Induced Formation of DNA Three-Way Junctions and Its Application to Protein Detection and DNA Strand Displacement. *Anal. Chem.* **2013**, *85*, 10835–10841.
- (25) Chen, X. Expanding the Rule Set of DNA Circuitry with Associative Toehold Activation. *J. Am. Chem. Soc.* **2012**, 134, 263–271.

- (26) Wang, B.; Thachuk, C.; Ellington, A. D.; Winfree, E.; Soloveichik, D. Effective design principles for leakless strand displacement systems. *Proc. Natl. Acad. Sci. U. S. A.* **2018**, *115*, E12182–E12191.
- (27) Srinivas, N.; Ouldridge, T. E.; Šulc, P.; Schaeffer, J. M.; Yurke, B.; Louis, A. A.; Doye, J. P. K.; Winfree, E. On the biophysics and kinetics of toehold-mediated DNA strand displacement. *Nucleic Acids Res.* **2013**, *41*, 10641–10658.
- (28) Chen, R. P.; Blackstock, D.; Sun, Q.; Chen, W. Dynamic protein assembly by programmable DNA strand displacement. *Nat. Chem.* **2018**, *10*, 474–481.
- (29) Cui, L.; Zhou, J.; Yang, X.-Y.; Dong, J.; Wang, X.; Zhang, C. Catalytic hairpin assembly-based electrochemical biosensor with tandem signal amplification for sensitive microRNA assay. *Chem. Commun.* **2020**, *56*, 10191–10194.
- (30) Hunt, V. M.; Chen, W. A microRNA-gated thgRNA platform for multiplexed activation of gene expression in mammalian cells. *Chem. Commun.* **2022**, *58*, *62*15–*62*18.